Single-Shot Correlations and Two-Qubit Gate of Solid-State Spins

K. C. Nowack, *et al.*

Science **333**, 1269 (2011);
DOI: 10.1126/science.1209524

variation of the cavity coupling. Figure 4 shows the effective cooperativity thus extracted at an antinode $\tilde{\eta}$ versus $\langle n_c \rangle$. Because the control Rabi frequency is given by $\Omega_c = 2g\sqrt{n_c + 1}$, we expect a linear dependence of $\tilde{\eta}$ on $\langle n_c \rangle$ with a slope m equal to the y-axis intercept $\tilde{\eta}_0$. A linear fit to the data for $\langle n_c \rangle > 2$, where the atom-induced cavity line broadening has negligible effect, yields $m = 3.7 \pm 0.1$, $\tilde{\eta}_0 = 5 \pm 1$, and the ratio $\tilde{\eta}_0/m = 1.4 \pm 0.3$, in reasonable agreement with the model that predicts $m = \tilde{\eta}_0 = f_{eg}\eta_0 = 3.4$. The upper inset shows the peak transparency Θ versus $\langle n_c \rangle$. The transparency is defined as $\Theta = (T' - T)/(1 - T)$, where T' (T) denotes the resonant transmission with (without) the control field, and $T = \exp(-\mathcal{N}) = 0.67$. This plot shows that a substantial transparency increase over the vacuum-control level already occurs for one intracavity photon. In the future, it should be possible to use this effect in such applications as nondestructive measurement of the intracavity photon number (*20*, *21*).

We have demonstrated that a vacuum field can generate a transparency window in an ensemble of three-level atoms and observed the associated group delay. By using a cavity-enhanced control field, we could substantially modify the transmission of an atomic ensemble with ~10 control photons. We also note that two probe beams, even when passing through spatially separated regions of the atomic ensemble, should influence each other's group velocity through the common interaction with the cavity mode, paving the way to cavity-mediated strong photon-photon interaction and quantum gates (*1*, *2*). In such a geometry, the technical roadblocks associated with both cavity-coupling losses (*2*, *6*, *7*, *9*) and motional and state control of single atoms (*8*, *29*) are bypassed. More generally, this work offers the prospect of strongly nonlinear, multimode quantum optics, with a realistic outlook for advanced quantum devices operating coherently with single photons.

References and Notes

1. T. Pellizzari, S. A. Gardiner, J. I. Cirac, P. Zoller, *Phys. Rev. Lett.* **75**, 3788 (1995).
2. Q. A. Turchette, C. J. Hood, W. Lange, H. Mabuchi, H. J. Kimble, *Phys. Rev. Lett.* **75**, 4710 (1995).
3. A. Rauschenbeutel *et al.*, *Phys. Rev. Lett.* **83**, 5166 (1999).
4. D. Chang *et al.*, *Nat. Phys.* **4**, 884 (2008).
5. G. Rempe, R. J. Thompson, R. J. Brecha, W. D. Lee, H. J. Kimble, *Phys. Rev. Lett.* **67**, 1727 (1991).
6. R. J. Thompson, G. Rempe, H. J. Kimble, *Phys. Rev. Lett.* **68**, 1132 (1992).
7. P. Münstermann, T. Fischer, P. Maunz, P. W. H. Pinkse, G. Rempe, *Phys. Rev. Lett.* **82**, 3791 (1999).
8. K. M. Birnbaum *et al.*, *Nature* **436**, 87 (2005).
9. I. Fushman *et al.*, *Science* **320**, 769 (2008).
10. S. E. Harris, *Phys. Rev. Lett.* **62**, 1033 (1989).
11. S. Harris, Y. Yamamoto, *Phys. Rev. Lett.* **81**, 3611 (1998).
12. M. Fleischhauer, A. Imamoglu, J. Marangos, *Rev. Mod. Phys.* **77**, 633 (2005).
13. K.-J. Boller, A. Imamolu, S. E. Harris, *Phys. Rev. Lett.* **66**, 2593 (1991).
14. M. M. Kash *et al.*, *Phys. Rev. Lett.* **82**, 5229 (1999).
15. L. V. Hau, S. E. Harris, Z. Dutton, C. H. Behroozi, *Nature* **397**, 594 (1999).
16. M. Bajcsy *et al.*, *Phys. Rev. Lett.* **102**, 203902 (2009).
17. J. E. Field, *Phys. Rev. A* **47**, 5064 (1993).
18. P. R. Rice, R. J. Brecha, *Opt. Commun.* **126**, 230 (1996).
19. G. Nikoghosyan, M. Fleischhauer, *Phys. Rev. Lett.* **105**, 013601 (2010).
20. C. Guerlin *et al.*, *Nature* **448**, 889 (2007).
21. D. I. Schuster *et al.*, *Nature* **445**, 515 (2007).
22. M. Mücke *et al.*, *Nature* **465**, 755 (2010).
23. T. Kampschulte *et al.*, *Phys. Rev. Lett.* **105**, 153603 (2010).
24. H. Tanji-Suzuki *et al.*, arxiv:quant-ph/1104.3594 (2011).
25. S. Gupta, K. L. Moore, K. W. Murch, D. M. Stamper-Kurn, *Phys. Rev. Lett.* **99**, 213601 (2007).
26. F. Brennecke *et al.*, *Nature* **450**, 268 (2007).
27. Y. Colombe *et al.*, *Nature* **450**, 272 (2007).
28. V. Vuletić, C. Chin, A. J. Kerman, S. Chu, *Phys. Rev. Lett.* **81**, 5768 (1998).
29. S. Nußmann *et al.*, *Phys. Rev. Lett.* **95**, 173602 (2005).

Acknowledgments: Supported by NSF grant PHY-0855052, the NSF-funded Center for Ultracold Atoms (grant PHY-0551153), and the Defense Advanced Research Projects Agency (QuASAR program) through the Army Research Office.

9 May 2011; accepted 12 July 2011
Published online 4 August 2011;
10.1126/science.1208066

Single-Shot Correlations and Two-Qubit Gate of Solid-State Spins

K. C. Nowack,[1]* M. Shafiei,[1] M. Laforest,[1]† G. E. D. K. Prawiroatmodjo,[1] L. R. Schreiber,[1] C. Reichl,[2] W. Wegscheider,[2] L. M. K. Vandersypen[1]*

Measurement of coupled quantum systems plays a central role in quantum information processing. We have realized independent single-shot read-out of two electron spins in a double quantum dot. The read-out method is all-electrical, cross-talk between the two measurements is negligible, and read-out fidelities are ~86% on average. This allows us to directly probe the anticorrelations between two spins prepared in a singlet state and to demonstrate the operation of the two-qubit exchange gate on a complete set of basis states. The results provide a possible route to the realization and efficient characterization of multiqubit quantum circuits based on single quantum dot spins.

For the efficient implementation and characterization of quantum information protocols, the ability to measure multiple qubits individually and in a single-shot manner is crucial (*1*, *2*). The key reason is that output states are often entangled quantum superpositions. If only one qubit is read out after every protocol run, the protocol must be repeated to measure successive bits, the superposition may collapse to a different state after every run, and correlations between the bits will possibly be lost. Joint measurements that require averaging over many runs pose similar problems, as various collapses contribute to the result. In contrast, independent single-shot measurement of all qubits gives full information from one collapse, which means that information contained in the (quantum) correlations can be obtained in the measurement.

A promising platform for realizing quantum protocols is provided by spins in the solid state, as they are well-isolated from the environment yet can be well controlled (*3*, *4*). Spin detection has been pushed to the single-spin level with the use of magnetic resonance force microscopy (*5*), scanning tunneling microscopy (*6*, *7*), optical spectroscopy (*8*–*10*), and transport spectroscopy (*11*–*13*).

Single-shot read-out of individual spins requires accumulation of a signal sufficiently strong to distinguish two spin states before the spin decays. Electrical single-shot read-out of a single electron spin has been realized in gate-defined quantum dots (*14*, *15*) and for a P impurity in Si (*16*). Optical single-shot read-out was achieved for a nuclear spin next to a diamond nitrogen-vacancy center (*17*) and for an electron spin in a self-assembled quantum dot (*18*). On two-electron systems, electrical single-shot read-out has been demonstrated as well (*19*, *20*), but only one bit of information was obtained on the joint state of the two spins.

Extending existing methods to independent read-out of two spins is not trivial: (i) Measurement of the first spin must be sufficiently noninvasive to allow subsequent measurement of the other. (ii) Independent read-out requires a vanishing coupling between the two spins, whereas a finite coupling is required for universal control of the spins. (iii) While the first spin is being measured, the second spin is subject to relaxation, which places tight restrictions on the read-out duration, hence the signal-to-noise ratio.

Here we demonstrate independent single-shot read-out of two electron spins in a double quantum dot, show that there is negligible cross-talk between the two measurements, and probe the correlations between the respective measurement outcomes for a variety of input states. The read-out allows us to demonstrate and benchmark the operation of the two-qubit exchange gate on a complete set of input states.

Our double quantum dot is formed by using Ti/Au surface gates to locally deplete a two-

[1]Kavli Institute of Nanoscience, Delft University of Technology, Post Office Box 5046, 2600 GA Delft, Netherlands. [2]Solid State Physics Laboratory, ETH Zurich, Schafmattstrasse 16, 8093 Zurich, Switzerland.

*To whom correspondence should be addressed. E-mail: k.c.nowack@tudelft.nl (K.C.N.), l.m.k.vandersypen@tudelft.nl (L.M.K.V.)

†Present address: Institute for Quantum Computing, University of Waterloo, Waterloo, Ontario, N2L 3G1 Canada.

dimensional electron gas 90 nm below the surface of a GaAs/(Al,Ga)As heterostructure (Fig. 1A, inset). We tune the device to the few-electron regime (Fig. 1A) and adjust the tunnel coupling between the dots and to the leads via the gate voltages. In all measurements, the inter-dot tunnel coupling ranges from 2 to 8 μeV, determined by microwave spectroscopy (*21*). Quantum point contacts (QPCs) on both sides of the structure allow us to monitor the charge occupation of the double dot. We used room-temperature IV converters to record the current from the left and right QPCs ($I_{QPC}^{L,R}$), and we monitored it in real time (*22*) so that individual electrons can be seen to leave and enter the dots. To set the electrochemical potentials in the left and right dot independently, we used combinations of voltages on gates left plunger (LP) and right plunger (RP), which compensate for capacitive cross-coupling. An in-plane magnetic field $B_{ext} = 6.5$ T is applied to split the spin-up (↑) and spin-down (↓) energy of both electrons by the Zeeman energy ($E_Z \approx 130$ μeV) defining a qubit in each of the dots. The electron temperature is typically 250 mK.

The read-out protocol consists of two steps (Fig. 1, B and C). Starting with one electron in each dot, the spin in the right dot is read out by applying a gate voltage pulse, which lines up the chemical potentials for spin-up and spin-down just below and above the Fermi level in the reservoir (position 1 in Fig. 1, A and B). A spin-up electron will then remain in the dot as it does not have enough energy to reach the unoccupied states in the reservoir, but a spin-down electron will tunnel out; soon afterwards, the dot will be refilled with a spin-up electron (*14*). Throughout this process, the QPC current is monitored. From a flat QPC response, we infer the electron was ↑; if the response shows a step, we conclude the electron was ↓ (Fig. 1C) [see supporting online material (SOM) text for details on the threshold analysis]. Subsequently, the spin in the left dot is read out in a similar manner (position 2 in Fig. 1, A and B) (*23*).

Each single-shot measurement trace contains two segments, reflecting the spin states of the right and left dot, respectively (Fig. 1C). Because we can read out both spins starting from the same state preparation, the measurement protocol achieves independent single-shot read-out of two solid-state spins. By construction, the read-out protocol resets both qubits to ↑.

As a first test of the measurement protocol, we inject a random spin in each of the dots by emptying the dot and then rapidly pulsing the levels down (Fig. 1D). We then wait in the (1,1) charge region for a variable time and read out

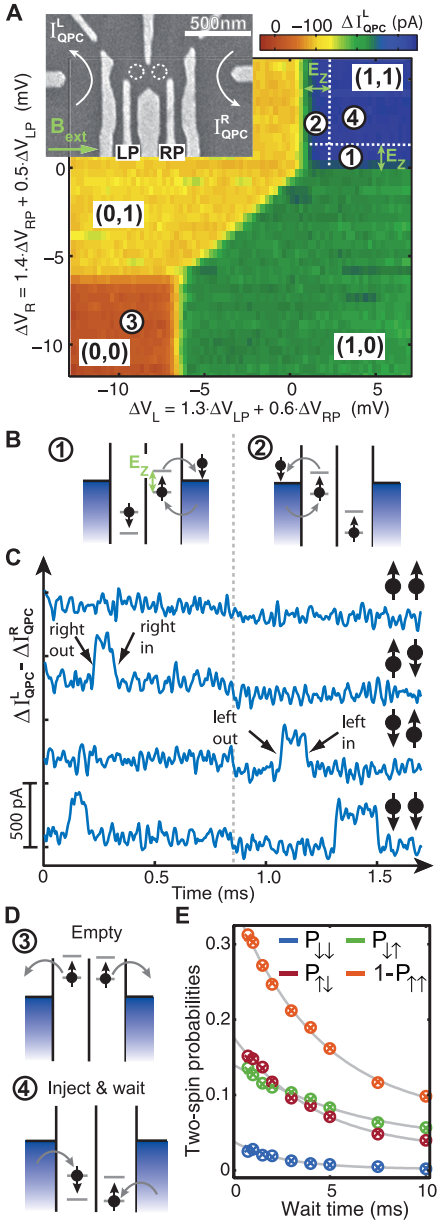

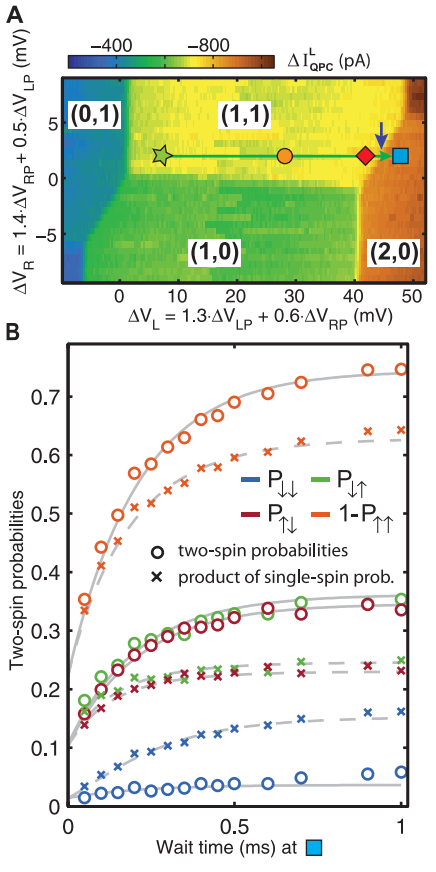

Fig. 1. (**A**) Charge stability diagram, with I_{QPC}^{L} shown in color scale as a function of voltages applied to gates LP and RP (a background plane has been subtracted). The occupation in the left and right dots is indicated by numbers in brackets. (Inset) Scanning electron micrograph of a device similar to the one used in our experiment. Gates LP and RP are connected to high-frequency lines via bias-tees. The direction of B_{ext} is indicated. (**B**) Electrochemical potential diagrams showing the double-dot configuration in the two read-out stages [positions (1) and (2) in (A)]. Tunnel events that occur for a ↓↓ state are indicated. (**C**) Single-shot read-out traces, displaying the difference of the current through the two QPCs, which are oppositely biased (22). The first and second parts correspond to read-out of the right and left dots, respectively. Four typical responses are shown (offset for clarity), one for each of the possible two-spin states. (**D**) Diagrams illustrating initialization into a random spin state [positions (3) and (4) in (A)]. (**E**) Measured probabilities to find the spin states ↑↑, ↑↓, ↓↑, and ↓↓ as a function of wait time before the read-out. Circles denote two-spin probabilities; crosses and gray lines indicate the product of single-spin probabilities (e.g., $P_{\uparrow}^{L} \cdot P_{\downarrow}^{R}$ for ↑↓), where the lines are based on exponential fits to the single-spin probabilities, with fitted spin relaxation times, T_1, in the left and right dot of 4.9 ± 1.7 ms and 3.8 ± 0.7 ms, respectively (see fig. S3).

Fig. 2. (**A**) Charge stability diagram including the (2,0) charge region. Symbols indicate positions relevant for the measurements shown in (B), as well as in Figs. 3 and 4. (**B**) Two-spin probabilities as a function of wait time in the (2,0) charge region at the position of the blue square in (A). Circles and solid gray lines denote two-spin probabilities; crosses and dashed gray lines indicate products of single-spin probabilities. The solid gray lines are exponentials with saturation values determined by the two-spin probabilities calculated from independently determined read-out fidelities (see SOM text) and the ideal values $P_{\uparrow\uparrow} = P_{\downarrow\downarrow} = 0, P_{\uparrow\downarrow} = P_{\downarrow\uparrow} = 1/2$. The time constant is determined from an exponential fit to the $P_{\uparrow\uparrow}$ data, and the initial values account for the spin-up and spin-down injection probabilities.

both spins. Repeating these steps, we collect statistics and determine the two-spin probabilities $P_{\uparrow\uparrow}$, $P_{\uparrow\downarrow}$, $P_{\downarrow\uparrow}$, and $P_{\downarrow\downarrow}$. As expected because of relaxation at low temperature, the ground-state probability $P_{\uparrow\uparrow}$ increases exponentially, at the expense of the three other probabilities (Fig. 1E). Given the injection of random spins in each of the dots [the actual probability for injecting spin-down is typically only 25 to 30%, depending on where the electrons are injected (*24*)], the probabilities should not display any correlations. Indeed, the products of the single-dot probabilities—for example, $P_{\downarrow}^{L} = P_{\downarrow\uparrow} + P_{\downarrow\downarrow}$—overlap with the corresponding two-spin probabilities (circles versus crosses in Fig. 1E), as expected for uncorrelated spins.

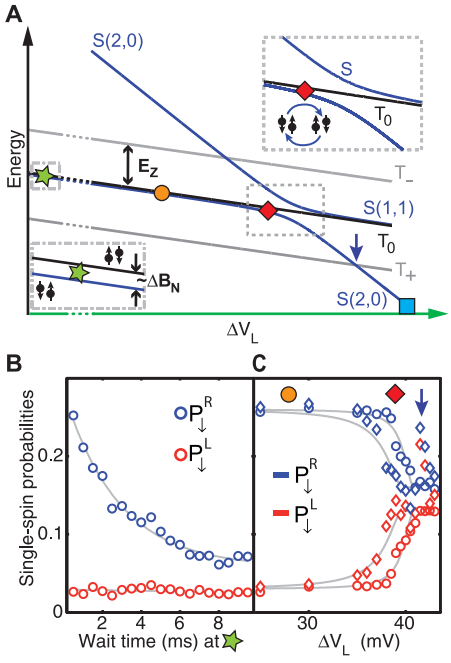

Fig. 3. (**A**) Schematic of the energy levels close to the (1,1)-(2,0) boundary, along the green arrow in Fig. 2A. Due to the Pauli exclusion principle, the ground state in the (2,0) charge region is a spin singlet. The (1,1) and (2,0) charge states with the same spin hybridize due to the inter-dot tunnel coupling. $S(1,1)$ and $S(2,0)$ denote the spin singlets in the (1,1) and (2,0) charge configuration. T_+, T_0, and T_- are the three (1,1) triplets with magnetic quantum number = +1, 0, and −1. T_+ and T_- are split off due to B_{ext}. (**B**) Single-spin probabilities to find ↓ as a function of wait time at the position of the green star (see also Fig. 2A) when initializing the left spin deterministically in ↑ and the right spin in a random spin state. (**C**) After initialization as in (B), the double dot is pulsed for 25 ns (circles) or 10 μs (diamonds) to a position close to the (1,1)-(2,0) charge transition. Single-spin probabilities to find ↓ as a function of this position are shown. Gray lines are a guide for the eye.

Correlations between the states of the two spins are induced when after injection of random spins in (1,1), we pulse into the (2,0) charge region for a variable time (Fig. 2A), during which relaxation to the (2,0) spin-singlet ground state will take place. When we subsequently separate the two electrons by pulsing into the (1,1) charge region and measure both spins, we see that correlations build up in the measurement outcomes consistent with singlet preparation [random local nuclear fields may dephase the singlet, but the antiparallel correlations survive (*25*)]: Whenever measurement of the left dot gives a spin-up outcome, measurement of the right dot most likely gives spin-down, and vice versa (Fig. 2B).

The (anti-)correlations are further elucidated by comparing the four two-spin probabilities (circles in Fig. 2B) with the product of the respective single-spin probabilities (crosses). For each spin by itself, the spin-down probability is ideally 1/2. However, the joint probability for ↓↓ is not 1/2 × 1/2 = 1/4, but instead 0. This gap between circles and crosses develops in Fig. 2B as the singlet probability increases. The deviation from the ideal values is quantitatively understood on the basis of the estimated read-out fidelities (gray lines, see below and SOM text). This demonstrates that the joint single-shot read-out allows us to directly probe correlations between two spins.

We next examine whether the read-out of both spins is truly independent, in the sense that the measurement outcome of one spin is not influenced by the measurement and/or the state of the other spin. First, with proper alignment of the respective chemical potentials (Fig. 1B) and sufficiently small QPC bias (typically 400 μeV) (*26*), one electron stays in its dot while the other is being measured. A more subtle possible cross-talk effect is that the second dot will not be lined up in the proper read-out configuration if the first dot is empty (due to the cross-capacitance). We therefore discard those traces (here, <5%) where the right dot was emptied but not refilled during the first read-out stage (see SOM text and fig. S2).

The most relevant remaining possible origin of cross-talk arises from the tunnel coupling between the dots, which results in exchange coupling of the two spins. To address this issue, we initialize the left spin deterministically in ↑ by waiting sufficiently long in the (1,0) charge region for the spin to relax. Subsequently, we inject an electron with random spin into the right dot, at gate settings for which (1,0) is lower in energy than (0,1) so the left electron stays in its dot while the right electron tunnels in. We observe no decay for the left dot (Fig. 3B), whereas the right dot shows the usual exponential decay. From the amplitude of this exponential decay compared to the standard deviation of the red data points in

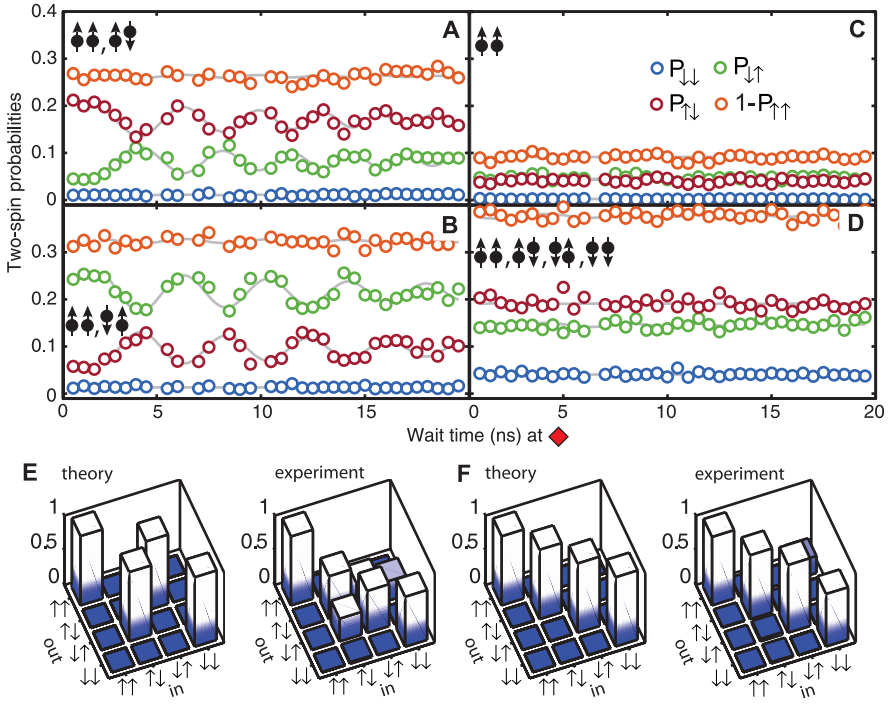

Fig. 4. (**A** to **D**) Two-qubit exchange gate on a full set of input states. The four panels correspond to four different mixtures of initial states, as indicated, taken with otherwise identical settings. Again, spin-down injection probabilities are below 50%. Gray lines are fits to damped oscillations, including a correction for pulse imperfections. We first fit $P_{\uparrow\downarrow}$ in (A) and $P_{\downarrow\uparrow}$ in (B) and allow only the amplitude and offset of the oscillations to change for the other probabilities in the respective panel. In (C) and (D), we use the fit parameters of (A) and allow only amplitude and offset to change. The oscillations in (A) and (B) run out of phase with each other for longer wait times. We attribute this to subtle distortions of the pulses arriving at the sample due to the bias tees (*22*). (**E** and **F**) Visualized theoretical and experimental truth tables for a π rotation and a 2π rotation of the exchange oscillation (details and actual numbers are given in the SOM and fig. S5).

Fig. 3B, the probability of exchange during the waiting interval between injection and read-out can be bounded to <2% (the read-out positions are at similar detuning, which gives a similar bound on exchange during read-out). Similar results are obtained when the order of the two read-out segments is reversed, as well as for other choices of initialization. In all cases, within the limits of our detection, the results confirm independent read-out of the two spins.

Cross-talk through electron-spin exchange is absent because the waiting and read-out positions in the (1,1) region are chosen close to both the (1,0) and (0,1) regions, where the random nuclear fields dominate over the exchange coupling between the spins (*25*). Therefore, the energy eigenbasis is ↑↑, ↑↓, ↓↑, and ↓↓, which coincides with the measurement basis (Fig. 3A, left inset). When we move the position of the waiting interval toward the (1,1)-(2,0) boundary along the green arrow in Fig. 2A, the exchange splitting increases, and eventually the eigenstates are given by the two-electron singlet and triplet states (Fig. 3A). The effect on the read-out fidelity is visible from Fig. 3C, where the populations of the left and right dots begin to mix if the waiting time is shifted too far or for too long toward the (1,1)-(2,0) boundary (which we took advantage of for creating singlet correlations in Fig. 2B). Exactly at the boundary between (1,1) and (2,0) (dark blue arrow in Figs. 2A and 3A) we observe an enhanced spin-down probability in both dots for the 10-μs wait time. At this position, the triplet with both spins up (T_+) and the singlet (S) cross and mix on a time scale of hundreds of nanoseconds.

Independent two-spin read-out also permits us to benchmark two-qubit gates. Here, we specifically address the SWAP gate, obtained through half a period of an exchange oscillation of the two spins. This oscillation can be observed by varying the wait time at a point close to the (1,1)-(2,0) boundary (Fig. 3A, right inset). Exchange oscillations have previously been shown in measurements relying on Pauli spin blockade for detection and state initialization (*25*), which suffices to demonstrate a single-qubit gate acting on a S-T_0 qubit (*27*). Here, we are able to verify the full operation of the two-qubit exchange gate acting on a set of input states covering the entire two-spin Hilbert space (*28*).

When initializing in a mixture of ↑↑ and ↑↓, we clearly observe the oscillation of the ↑↓ probability (Fig. 4A). Different from all previous measurements (*25*, *29*), we also obtain the ↓↑ probability, which oscillates in antiphase, as well as the ↑↑ and ↓↓ probabilities, which, as expected, do not vary with exchange time (Fig. 4A). Similar measurements for three other initial states are shown in Fig. 4, B to D, in all cases giving the predicted behavior for the evolution under the exchange Hamiltonian. Together these measurements cover a complete set of input states for the two-qubit exchange gate, which allows us to establish a "truth table" (we did not perform process tomography, which requires measurements in different bases), which expresses with what probability the gate maps the four basis states onto each other (Fig. 4, E and F).

To obtain this truth table, we first need to analyze the read-out fidelities. In the absence of cross-talk, the main processes contributing to read-out errors are that (i) a spin-up electron can tunnel out of the dot due to thermal or other excitations, (ii) a spin-down electron may not tunnel out but instead relax to spin-up and (iii) the dot may refill so quickly after a spin-down electron tunnels out, that the step is not observed because of the finite detection bandwidth. Therefore, we carefully made trade-offs in the QPC bias, analysis threshold, the duration of each read-out, the transparency of the tunnel barriers and the strength of the magnetic field [which affects not only the Zeeman splitting but also T_1 (*14*, *30*)]. For the (near-optimal) settings of Fig. 4, we get fidelities of 95.7 ± 0.4% and 95.0 ± 0.5% for ↑ in the right and left dot, and 77.7 ± 0.9% and 78.0 ± 4% for ↓ in the right and left dot (see supporting online text for a detailed discussion of the error processes). This gives a read-out fidelity of 86 ± 1% on average.

From the data in Fig. 4, A to D, and the estimated read-out fidelities, we construct the truth table for half a period of the exchange oscillation (Fig. 4E) (SOM text), which should produce a two-qubit SWAP gate. The data shows that the spins are only partly exchanged. To gain more insight into what limits the SWAP fidelity, we also consider the truth table of a full period of the oscillation (Fig. 4F). This operation ideally corresponds to unity, and the measured map matches this expectation. This suggests that the SWAP fidelity is not limited by fluctuations of the exchange strength, as caused, for instance, by charge noise or gate voltage noise. Instead, the dominant errors may be due to local nuclear fields, which tilt the rotation axis (*29*), and the limited rise time of the voltage pulse, which makes the passage from the read-out region to the SWAP operation point and back partly adiabatic. Whereas a more detailed analysis is beyond the scope of this work, the two independent spin read-outs offer a powerful tool for characterizing and benchmarking two-spin gates and for providing guidance to improving gate performance.

The independent single-shot read-out of two spins allows us to directly observe the correlations between two spins initialized in a singlet state and to characterize the full exchange gate between neighboring spins. Cross-talk between the two measurements is negligible. The average read-out fidelity is typically estimated to be 86% and can be substantially improved by implementing more sensitive charge detection (*31*, *32*) or measuring at lower magnetic field (*14*, *30*), which requires a lower electron temperature or additional dots (*33*). Our results suggest that multiple-qubit measurement in quantum dots is possible, providing a route for the realization of quantum algorithms and quantum error correction codes with solid-state spins.

References and Notes

1. M. Nielsen, I. Chuang, *Quantum Computation and Information* (Cambridge Univ. Press, Cambridge, 2000).
2. P. W. Shor, in *Proceedings of 35th Annual Symposium on Foundations of Computer Science* (IEEE Press, Los Alamitos, CA, 1994), pp. 124–134 (1994).
3. R. Hanson, L. P. Kouwenhoven, J. R. Petta, S. Tarucha, L. M. K. Vandersypen, *Rev. Mod. Phys.* **79**, 1217 (2007).
4. R. Hanson, D. D. Awschalom, *Nature* **453**, 1043 (2008).
5. D. Rugar, R. Budakian, H. J. Mamin, B. W. Chui, *Nature* **430**, 329 (2004).
6. A. J. Heinrich, J. A. Gupta, C. P. Lutz, D. M. Eigler, *Science* **306**, 466 (2004); 10.1126/science.1101077.
7. F. Meier, L. Zhou, J. Wiebe, R. Wiesendanger, *Science* **320**, 82 (2008).
8. F. Jelezko, T. Gaebel, I. Popa, A. Gruber, J. Wrachtrup, *Phys. Rev. Lett.* **92**, 076401 (2004).
9. J. Berezovsky *et al.*, *Science* **314**, 1916 (2006); 10.1126/science.1133862.
10. M. Atatüre, J. Dreiser, A. Badolato, A. Imamoglu, *Nat. Phys.* **3**, 101 (2007).
11. R. Hanson *et al.*, *Phys. Rev. Lett.* **91**, 196802 (2003).
12. R. M. Potok *et al.*, *Phys. Rev. Lett.* **91**, 016802 (2003).
13. H. Sellier, G. P. Lansbergen, J. Caro, S. Rogge, *Phys. Rev. Lett.* **97**, 206805 (2006).
14. J. M. Elzerman *et al.*, *Nature* **430**, 431 (2004).
15. C. B. Simmons *et al.*, *Phys. Rev. Lett.* **106**, 156804 (2011).
16. A. Morello *et al.*, *Nature* **467**, 687 (2010).
17. P. Neumann *et al.*, *Science* **329**, 542 (2010); 10.1126/science.1189075.
18. A. N. Vamivakas *et al.*, *Nature* **467**, 297 (2010).
19. R. Hanson *et al.*, *Phys. Rev. Lett.* **94**, 196802 (2005).
20. C. Barthel, D. J. Reilly, C. M. Marcus, M. P. Hanson, A. C. Gossard, *Phys. Rev. Lett.* **103**, 160503 (2009).
21. T. H. Oosterkamp *et al.*, *Nature* **395**, 873 (1998).
22. Materials and methods are available as supporting material on *Science* Online.
23. We can also bring both dots into the read-out configuration simultaneously, making read-out faster but signal analysis more challenging, as tunneling from the left versus right dot must be distinguished.
24. S. Amasha *et al.*, *Phys. Rev. B* **78**, 041306 (2008).
25. J. R. Petta *et al.*, *Science* **309**, 2180 (2005); 10.1126/science.1116955.
26. D. Taubert *et al.*, *Phys. Rev. Lett.* **100**, 176805 (2008).
27. J. Taylor *et al.*, *Nat. Phys.* **1**, 177 (2005).
28. D. Loss, D. P. DiVincenzo, *Phys. Rev. A* **57**, 120 (1998).
29. S. Foletti, H. Bluhm, D. Mahalu, V. Umansky, A. Yacoby, *Nat. Phys.* **5**, 903 (2009).
30. A. Khaetskii, Y. Nazarov, *Phys. Rev. B* **64**, 125316 (2001).
31. D. Reilly, C. Marcus, M. Hanson, A. Gossard, *Appl. Phys. Lett.* **91**, 162101 (2007).
32. C. Barthel *et al.*, *Phys. Rev. B* **81**, 161308 (2010).
33. H.-A. Engel *et al.*, *Phys. Rev. Lett.* **93**, 106804 (2004).

Acknowledgments: We thank P. Barthelemy, F. Braakman, L. DiCarlo, S. Frolov, R. Hanson, E. Laird, J. Mooij, and P. Scarlino for useful discussions; R. Schouten for electronics support; P. de Groot and R. Heeres for help with the measurement software; and A. van der Enden, J. Haanstra, and R. Roeleveld for general technical support. We acknowledge funding from the Intelligence Advanced Research Projects Activity through the Army Research Office, the Dutch Foundation for Fundamental Research on Matter, the European Research Council (ERC starting grant), and the European Commission (SOLID). C.R. and W.W. acknowledge financial support by the Swiss National Science Foundation. M.L. acknowledges support from Le Fonds Québécois de la Recherche sur la Nature et les Technologies.

Supporting Online Material

www.sciencemag.org/cgi/content/full/science.1209524/DC1
Materials and Methods
SOM Text
Figs. S1 to S5
References (*34*, *35*)

8 June 2011; accepted 26 July 2011
Published online 4 August 2011;
10.1126/science.1209524